

Non-autonomous bright solitons and their stability in Rabi coupled binary Bose-Einstein Condensates

T Kanna[†], R Babu Mareeswaran[†], and Franz G Mertens[‡]

[†]Post Graduate and Research Department of Physics, Bishop Heber College, Tiruchirappalli-620 017, Tamil Nadu, India

[‡]Physikalisches Institut, Universität Bayreuth, D-95440 Bayreuth, Germany

E-mail: kanna_phy@bhc.edu.in (corresponding author), franzmertens@gmail.com

Abstract. The dynamics of non-autonomous bright matter-wave solitons in Rabi coupled binary Bose-Einstein condensates is explored. By performing a unitary and similarity/lens-type transformation, we reduce the non-autonomous Gross-Pitaevskii equation into the celebrated Manakov model. Then, we construct the exact bright solitons of the non-autonomous Gross-Pitaevskii system in the presence of time dependent nonlinearities for two specific forms, namely hyperbolic nonlinearities, which are of physical interest. The experimental possibilities of realizing the forms of temporally modulated potentials corresponding to these time dependent nonlinearities and supporting such localized structures are explored. Our study on the propagation of one soliton shows that the amplitude, velocity and shape of the bright soliton are altered by the time-dependent scattering length. We also analyse the non-trivial energy sharing collision of Manakov solitons in the presence of Rabi coupling and aforementioned nonlinearities. We find that breathers arise in two-soliton collisions and the nature of energy sharing collisions is altered from that of Manakov system due to Rabi coupling only. Further in the presence of time-dependent nonlinearities the collision scenario is again altered significantly. Finally, the stability of these localized structures is examined using a recently developed powerful analytic method by Quintero et. al., [Phys. Rev. E 91, 012905 (2015)] and it is shown that the non-autonomous bright solitons are indeed stable. The evolution of position and velocity is also studied.

PACS numbers: 05.45.Yv, 02.30.IK, 03.75.Lm, 03.75.-b

1. Introduction

Bose-Einstein condensates (BECs) have become an important ground for the study of macroscopic quantum phenomena [1]. Since the first realization of BECs with alkali atoms, various nonlinear structures have been experimentally observed and/or theoretically investigated, such as bright solitons [2], dark solitons [3], dark-bright solitons [4], vortices [5], Faraday waves [6], skyrmions [7], etc. BECs with tunable interatomic interactions have been the subject of intense theoretical and experimental interest in recent years [8]. In the vicinity of a Feshbach-resonance (FR), the atomic scattering length depends sensitively on the applied external magnetic field (see refs. [9, 10] and references therein), allowing the magnitude and sign of the atomic interactions to be tuned to any value. These techniques offer some opportunities to achieve a nonlinearity management through the use of time-dependent and/or nonuniform fields. Utilizing this nonlinearity management concept, several nonlinear wave patterns and effects, such as, non-autonomous bright solitons [11] as well as dark-bright solitons [12], Bloch oscillations [13], and rogue waves [14] have been observed in BECs.

Multicomponent BECs are a mixture of different atomic species (heteronuclear BEC mixtures) or a mixture of same species at different hyperfine states (homonuclear BEC mixtures). Of the multi-component BECs, the simplest form is the two-component BEC. In homonuclear BECs, in addition to the inter species interaction the two different hyperfine states can be coupled by ‘‘Rabi coupling’’. This is a linear coupling between separate wave functions say $|1\rangle$ and $|2\rangle$ induced by radio-frequencies. When the coupling drive is turned on, suddenly, it will induce an extended series of oscillations of the total population from the $|1\rangle$ to the $|2\rangle$ state, so called ‘‘Rabi oscillations’’ [15]. Under the application of Rabi coupling between the components of a weakly interacting multicomponent BECs, one component of BECs can be transferred to another [16, 17]. Experiments have been performed for two-component ^{87}Rb condensate with atomic states customarily denoted by $|1\rangle$ and $|2\rangle$; in particular, these states can be either $|F = 2, m_F = 1\rangle$ and $|2, 2\rangle$ [18], or $|1, -1\rangle$ and $|2, 1\rangle$ [15]. In a recent experimental work [19], solitons have been observed in a binary Gross-Pitaevskii (GP) system with Rabi coupling. Several other studies on Rabi coupled binary GP systems, namely magnetic solitons [20], dark soliton [21], domain walls [22], vortex pairs [23], countersuperflow [24], and topological defects [25], have also been investigated.

Motivated by these works, here we study theoretically the non-autonomous bright solitons and their stability in a Rabi-coupled quasi-one-dimensional GP system. In our earlier work, two of the authors (T.K. and R.B.) and co-workers considered the repulsive condensates and studied the dark-bright solitons dynamics. Now our attention is on attractive condensates and their soliton patterns, which are distinctly different from those observed in Ref. [12].

On the other hand, stability of nonlinear waves in multi-component BECs is another critical issue in $(1+1)$ - dimension as well as in higher dimensions. To the best of

our knowledge so far no analytical tool has been developed to study the stability of multi-component non-autonomous soliton like structures appearing in integrable non-autonomous nonlinear evolution equations. Recently, Quintero et al., [26] proposed an efficient method to determine the stability of bright solitons in both autonomous and non-autonomous settings of the nonlinear Schrödinger (NLS) equation. In this work, we apply that method to the obtained bright soliton solutions of the non-autonomous GP system (2) given below. The rest of the paper is organized as follows:

In section II, we describe the model equation for quasi one-dimensional Rabi-coupled BEC. In section III, we show that under a suitable unitary and similarity type transformation, the Rabi-coupled non-autonomous GP system can be converted into the famous integrable Manakov system along with a constraint condition. In section IV, we will study the evolution of one- and two-solitons in autonomous and non-autonomous Rabi-coupled GP systems and discuss their dynamical behavior for two particular physically interesting forms of the time-dependent nonlinearity coefficient. Following this, we address the stability of the obtained non-autonomous bright one-soliton by an analytical procedure developed recently by Quintero et al., [26] and show that the non-autonomous soliton structures reported here are indeed stable. Section VI contains the concluding remarks.

2. Description of the Model

We consider a two-component BEC that is condensed into two different hyperfine states $|1\rangle$ and $|2\rangle$ such as those of ^{87}Rb atoms [15]. The two component BEC is assumed to be trapped in a simple harmonic potential with the trapping in the transverse directions being stronger. Then the BEC is cigar-shaped and is governed by the following dimensionless one-dimensional (1D) GP equation [1]:

$$i\frac{\partial\psi_1}{\partial t} = \left[-\frac{1}{2}\frac{\partial^2}{\partial x^2} + V_{\text{ext}}(x, t) \right] \psi_1 + (g_{11}|\psi_1|^2 + g_{12}|\psi_2|^2)\psi_1 + \chi\psi_2, \quad (1a)$$

$$i\frac{\partial\psi_2}{\partial t} = \left[-\frac{1}{2}\frac{\partial^2}{\partial x^2} + V_{\text{ext}}(x, t) \right] \psi_2 + (g_{12}|\psi_1|^2 + g_{22}|\psi_2|^2)\psi_2 + \chi\psi_1. \quad (1b)$$

Here $\psi_j(x, t)$ ($j = 1, 2$) are the condensate wave functions in the two hyperfine states, spatial coordinate x and time t are respectively measured in units of a_0 and ω_{\perp}^{-1} , where $a_0 = \sqrt{\hbar/m\omega_{\perp}}$ (m denotes atomic mass) is the transverse harmonic oscillator length. The coupling constants $g_{ii} = 2a_{ii}/a_B$ for $i = 1, 2$ and $g_{12} = 2a_{12}/a_B$ are the intra-species and inter-species interaction strengths respectively, where a_B is the Bohr radius and a_{ij} are the s -wave scattering lengths of the species i and j respectively, and can be tuned with the aid of magnetic-field induced FR mechanism [27, 28]; $V_{\text{ext}}(x, t) = \frac{1}{2}\Omega^2(t)x^2$ (where $\Omega^2(t) = \omega_x^2(t)/2\omega_{\perp}^2$, in which ω_x and ω_{\perp} are the temporally modulated axial trap frequency and radial frequency) is the time-dependent harmonic trap potential. The cross coupling term χ is the Rabi coupling parameter and is assumed to be real and positive.

Based on experimental results pertaining to two-component ^{87}Rb BECs [29], we can assume that the scattering lengths to be equal, and also they can be tuned through FR [30]. Hence, we consider the GP system (1) with equal interaction strengths, i.e., $g_{11} = g_{12} = g_{22} = -\beta(t)$, where $\beta(t)$ is a positive function. The resulting equations can be expressed as

$$i\frac{\partial\psi_1}{\partial t} = \left[-\frac{1}{2}\frac{\partial^2}{\partial x^2} + V_{\text{ext}}(x, t) \right] \psi_1 - \beta(t)(|\psi_1|^2 + |\psi_2|^2)\psi_1 + \chi\psi_2, \quad (2a)$$

$$i\frac{\partial\psi_2}{\partial t} = \left[-\frac{1}{2}\frac{\partial^2}{\partial x^2} + V_{\text{ext}}(x, t) \right] \psi_2 - \beta(t)(|\psi_1|^2 + |\psi_2|^2)\psi_2 + \chi\psi_1. \quad (2b)$$

Next, we derive the continuity equation from the time-dependent GP equation (2). For this purpose, the coupled GP system (2a) and (2b) is multiplied by ψ_1^* and ψ_2^* respectively, and the complex conjugate equations of the coupled GP system (2a) and (2b) are multiplied respectively by ψ_1 and ψ_2 . Combining the resulting equations suitably, we get

$$\frac{\partial\rho}{\partial t} + \frac{\partial j}{\partial x} = 0 \quad (3)$$

where norm density $\rho = (|\psi_1|^2 + |\psi_2|^2)$, and momentum current density $j = (i/2)[(\psi_1^*\psi_{1,x} - \text{c.c.}) + (\psi_2^*\psi_{2,x} - \text{c.c.})]$. Here c.c denotes complex conjugation. The norm (N) of Eq. (2) is given by

$$\text{Norm} : N = \int_{-\infty}^{\infty} \rho \, dx. \quad (4a)$$

We also require the following physical quantities, namely field momentum and normalized momentum for the stability analysis of the non-autonomous solitons.

$$\text{Field Momentum} : p = \int_{-\infty}^{\infty} j(x, t) \, dx, \quad (4b)$$

$$\text{Normalized Momentum} : P = \frac{p}{N}. \quad (4c)$$

3. Transforming Rabi coupled non-autonomous GP system to the Manakov system

In a recent work [12], two of the authors (T.K. and R.B.) along with their co-workers have converted Eq. (2) with repulsive nonlinearity to the defocusing coupled NLS system, a known integrable system by employing two successive transformations. Here we consider Eq. (2) with focusing nonlinearity, i.e., $\beta(t) > 0$. First, we utilize the following unitary transformation [31]

$$\begin{pmatrix} \psi_1 \\ \psi_2 \end{pmatrix} = \begin{pmatrix} \cos(\chi t) & -i \sin(\chi t) \\ -i \sin(\chi t) & \cos(\chi t) \end{pmatrix} \begin{pmatrix} \Phi_1 \\ \Phi_2 \end{pmatrix}, \quad (5)$$

in Eq. (2). This special rotational transformation was first used in Ref. [31] to convert autonomous Rabi coupled GP system to standard coupled GP system. Following this in Ref. [12] we have applied this to transform non-autonomous Rabi coupled GP system to

defocusing GP system. Here the linearly (Rabi) coupled non-autonomous GP system (2) is transformed into a coupled non-autonomous GP system of defocusing type ($\beta(t) > 0$) without linear coupling [12]

$$i\frac{\partial\Phi_j}{\partial t} = -\frac{1}{2}\frac{\partial^2\Phi_j}{\partial x^2} - \beta(t)\sum_{l=1}^2(|\Phi_l|^2)\Phi_j + V_{\text{ext}}(x,t)\Phi_j, \quad j = 1, 2. \quad (6)$$

Next a proper similarity transformation is chosen in order to map the above non-autonomous GP system (6) to the celebrated Manakov system. The similarity transformation is given by

$$\Phi_j(x,t) = \varepsilon(t) Q_j(X(x,t), T(t)) \exp(i\phi(x,t)), \quad j = 1, 2. \quad (7)$$

Here, the co-ordinates $X(x,t) = \sqrt{2}\sigma_1(\beta(t)x - 2\sigma_2\sigma_1^2 \int \beta^2(t)dt)$, $T(t) = \sigma_1^2 \int \beta^2(t)dt$, $\varepsilon(t) = \sigma_1\sqrt{2\beta(t)}$, and $\phi(x,t) = -\frac{x^2}{2}\left(\frac{\dot{\beta}(t)}{\beta(t)}\right) + 2\sigma_1^2\sigma_2(\beta(t)x - \sigma_2\sigma_1^2 \int \beta^2(t)dt)$. The parameters σ_1 and σ_2 are arbitrary real constants. Inserting (7) into (6), we obtain

$$iQ_{1,T} + Q_{1,XX} + 2(|Q_1|^2 + |Q_2|^2)Q_1 = 0, \quad (8a)$$

$$iQ_{2,T} + Q_{2,XX} + 2(|Q_1|^2 + |Q_2|^2)Q_2 = 0, \quad (8b)$$

with the condition

$$(\ddot{\beta}/\beta) - 2(\dot{\beta}/\beta)^2 - \Omega^2(t) = 0. \quad (9)$$

The existence of such type of similarity transformation relating non-autonomous system to an integrable autonomous system was first proposed by Serkin [32] for the NLS system. Following this a flurry of activities [33] have been carried out along this direction. However the study of present system (2) with focusing nonlinearity is still left unexplored.

The similarity transformation between the linearly coupled non-autonomous GP system and the autonomous Manakov equation provides us an efficient way to construct the solutions of the Rabi coupled non-autonomous GP system from the known solutions of the Manakov system [34]. The bright one- and two- soliton solutions of the Manakov system (8) are obtained in Refs. [34, 35] are given in the appendix. In our earlier published work [12], we have investigated the dynamics of non-autonomous dark-bright one- and two- soliton solutions under Rabi coupling in the framework of a defocusing coupled NLS system. In the following section, with the knowledge of the bright one- and two-soliton solutions of the Manakov system (8) the non-autonomous bright soliton solutions of system (2) are obtained and their dynamical properties as well as their stability are discussed in detail. We would like to emphasize that the bright solitons of the Manakov system admit novel energy sharing collisions that have applications in optical computing [36, 37], matter wave interferometer [38], and partially coherent solitons [39, 40] of variable shape. Here we investigate these intriguing collisions in the presence of time dependent nonlinearity and Rabi coupling.

4. Forms of the time-dependent nonlinearity coefficients and their corresponding modulated trap frequencies

(a) First we choose a kink-like form of the nonlinearity coefficient, enabling the transition between two distinct (constant) values of β , namely,

$$\beta(t) = a_0 + \tanh(\rho t + \delta), \quad (10a)$$

where a_0 , ρ , and δ are arbitrary real constants. The associated form of strength of trap frequency $\Omega^2(t)$ is determined from Eq. (9)

$$\Omega^2(t) = -\frac{2\rho^2 \text{sech}^2(\rho t + \delta)(1 + a_0 \tanh(\rho t + \delta))}{a_1^2}, \quad (10b)$$

where $a_1 = a_0 + \tanh(\rho t + \delta)$.

The graphical structures of $\beta(t)$ and $\Omega^2(t)$ are shown in Fig. 1. It shows that the temporal modulation of the nonlinearity coefficient $\beta(t)$ (blue solid line) smoothly varies from one value (lower) to another value (higher) as time $t \rightarrow 0$ to 4., e.g., in atomic condensates such variations can be realized by tuning the magnetic field [41]. We depict the nature of the corresponding temporal modulation of the potential $\Omega^2(t)$ in the same figure as red solid lines. The form of $\Omega^2(t)$ agrees very well with the Hermite-Gaussian pulse $\gamma(t) = [c_0 H_0(\sigma) + c_3 H_3(\sigma)] \exp(-\sigma^2/2w^2)$, where $\sigma = 1.2t - 2.25$, w is the width of the Gaussian pulse, c_0 and c_3 are the coefficients of the zeroth order (H_0) and third order (H_3) Hermite polynomials, respectively. This is clearly shown in Fig. 1(b).

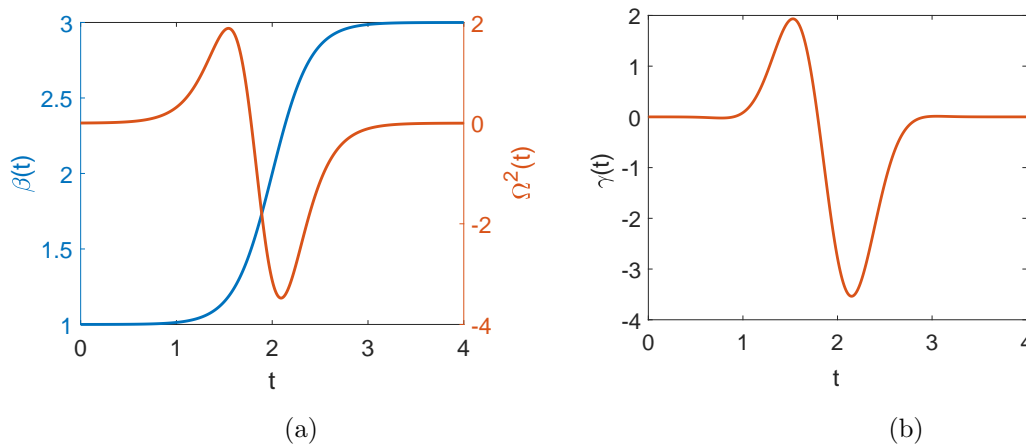


Figure 1. Panel (a): Profiles of nonlinearity $\beta(t)$ ($a_0 = 2$, $\rho = 0.5$ and $\delta = -5$) and trap frequency $\Omega^2(t)$ given by Eqs. (10a) and (10b), respectively. Panel (b): Typical plot of $\gamma(t)$ for $w = \sqrt{0.17}$, $c_0 = -1.2$, and $c_3 = 1$.

(b) We also choose another following form of variable nonlinearity coefficient to examines

$$\beta(t) = a_0 + \cosh(\rho t + \delta), \quad (11a)$$

where a_0 , δ and ρ are, again, real arbitrary constants, while the associated form of the trap frequency is found from Eq. (9) as

$$\Omega^2(t) = \frac{\rho^2[3 + 2a_0 \cosh(\rho t + \delta) - \cosh(2(\rho t + \delta))]}{2a_1^2}, \quad (11b)$$

where $a_1 = a_0 + \cosh(\rho t + \delta)$.

The graphical structures of $\beta(t)$ and $\Omega^2(t)$ are sketched in Fig. 2. The nature of time-dependent function $\beta(t)$ (blue solid line) admits a flat bottom parabolic profile (at $t = 0$ and 4 it reaches its maximum value, while $t = 2$ approaches its minimum value). Indeed it changes its value from negative to positive which can be very well achieved through FR mechanism. Next, the temporal modulation of the trap potential $\Omega^2(t)$ is found to be localized pulse, which can be experimentally realized. It is interesting to note that the nature of the above function $\Omega^2(t)$ well agrees with the function $\gamma(t) = aH_2(\sigma)\exp(-\sigma^2/2w^2)$, where $\sigma = t - 2$, a and w are the amplitude and width of the Gaussian pulse/beam, $H_2(\sigma)$ is the second order Hermite polynomial (see Fig. 2(b)). We believe that this resemblance of $\Omega^2(t)$ with Hermite-Gaussian (HG) pulse (second order) pointed out here, will pave way to realize non-autonomous solitons experimentally in multiple species condensates as these HG pulses can be formed by suitable laser sources.

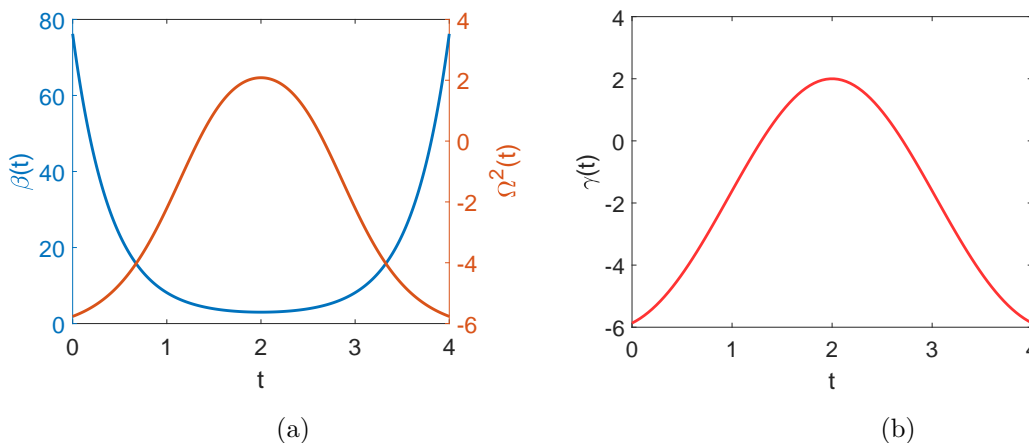


Figure 2. Panel (a): Profile of nonlinearity $\beta(t)$ ($a_0 = 2$, $\rho = 2.5$, and $\delta = -5$) and trap frequency $\Omega^2(t)$ given by Eqs. (11a) and (11b). Panel (b): Typical plot of $\gamma(t)$ for $w = \sqrt{2.3}$ and $a = -1$.

5. Explicit soliton solutions of non-autonomous coupled GP system

Here we write down the one- and two-soliton solutions of system (2) for constant as well as time-dependent nonlinearity coefficients. This will enable us to compare the dynamics of the bright solitons in the presence and absence of the time dependence of the nonlinearity coefficient β .

5.1. Bright one- soliton solution

(i) The bright one-soliton solution of system (2) for constant nonlinearity coefficient $\beta = 1$ and in the absence of an external potential $V_{\text{ext}}(x, t)$ is given by [35]

$$\psi_1(x, t) = (A_1 \cos(\chi t)Q_1 - iA_2 \sin(\chi t)Q_2), \quad (12a)$$

$$\psi_2(x, t) = (-iA_1 \sin(\chi t)Q_1 + A_2 \cos(\chi t)Q_2), \quad (12b)$$

where the functions Q_1 and Q_2 are given in Eq. (A.1) in the appendix. Here the variables ω and η_{1I} are redefined as $\omega = x - k_{1I}t$ and $\eta_{1I} = k_{1I}x + (k_{1R}^2 - k_{1I}^2)(t/2)$.

For constant nonlinearity coefficient (i.e., $\beta(t) = \text{const.}$) and in the absence of external potential ($V_{\text{ext}} = 0$, corresponding to homogeneous condensate), the soliton profiles in both the components $\psi_1(x, t)$ and $\psi_2(x, t)$ exhibit breathing (or) oscillating behavior due to the Rabi coupling parameter χ .

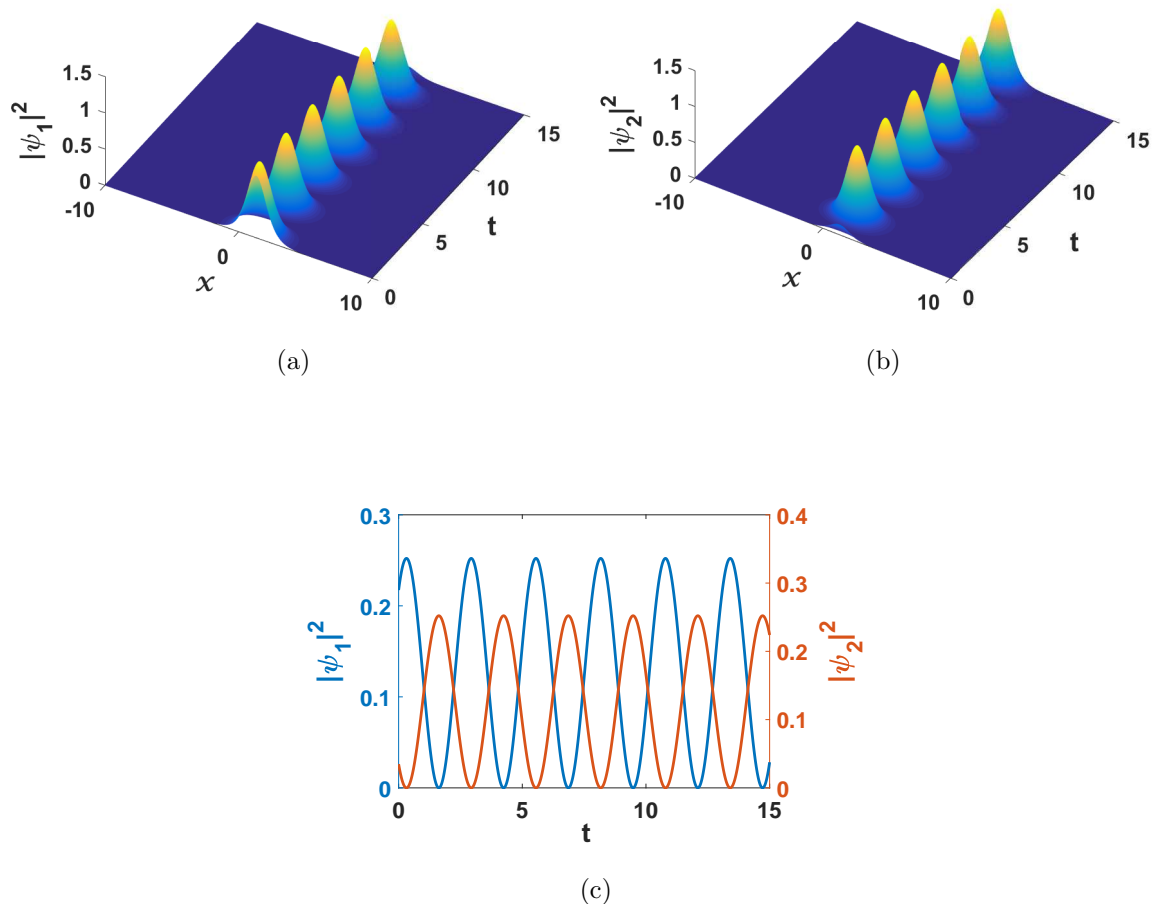


Figure 3. Oscillating soliton for constant nonlinearity coefficient $\beta(t)$ and in the absence of external potential. Panels (a) and (b) show contour plots of density profiles of $|\psi_1|^2$ and $|\psi_2|^2$. Panel (c) shows density profiles of $|\psi_1|^2$ and $|\psi_2|^2$. Here $k_{1R} = 1$, $k_{1I} = 0$, $\alpha_1^{(1)} = 0.5$, $\beta = 1$, $\alpha_1^{(2)} = 0.2i$, and $\chi = 1.2$.

Figs. 3(a)-3(c) show a train of identical breathing solitons/breathers. To facilitate the understanding of such oscillations we explicitly present the expressions for the condensate densities $|\psi_1|^2 = k_{1R}^2 \text{sech}^2(k_{1R}\omega + R/2)(|A_1|^2 \cos^2(\chi t) + |A_2|^2 \sin^2(\chi t)) + ik_{1R}^2 \cos(\chi t) \sin(\chi t) \text{sech}^2(k_{1R}\omega + R/2)(A_1 A_2^* - A_1^* A_2)$ and $|\psi_2|^2 = k_{1R}^2 \text{sech}^2(k_{1R}\omega + R/2)(|A_2|^2 \cos^2(\chi t) + |A_1|^2 \sin^2(\chi t)) + ik_{1R}^2 \cos(\chi t) \sin(\chi t) \text{sech}^2(k_{1R}\omega + R/2)(A_1^* A_2 - A_1 A_2^*)$. From this expression we find that the oscillations originate from the trigonometric functions (*cosine* and *sine*) appearing in the cross (interference) terms. The matter wave oscillation between the components becomes larger for large values of the Rabi coupling χ as expected.

(ii) The non-autonomous bright one-soliton solution of system (2) for time-dependent nonlinearity coefficient $\beta(t)$ and in the presence of external potential $V_{\text{ext}}(x, t)$ obtained by using the transformations mentioned in the previous section and the solution given in the appendix, is given below

$$\psi_1(x, t) = [A_1 \cos(\chi t) - iA_2 \sin(\chi t)] \varepsilon(t) k_{1R} \text{sech}(k_{1R}\tilde{\omega} + R/2) e^{i(\tilde{\eta}_{1I} + \phi(x, t))}, \quad (13a)$$

$$\psi_2(x, t) = [-iA_1 \sin(\chi t) + A_2 \cos(\chi t)] \varepsilon(t) k_{1R} \text{sech}(k_{1R}\tilde{\omega} + R/2) e^{i(\tilde{\eta}_{1I} + \phi(x, t))} \quad (13b)$$

where

$$\tilde{\omega} = X - 2k_{1I}T \quad (13c)$$

$$\tilde{\omega} = \sqrt{2}\sigma_1\beta(t)x - 2\sqrt{2}\sigma_1^3\sigma_2 \int \beta^2(t)dt - 2k_{1I}\sigma_1^2 \int \beta^2(t)dt, \quad (13d)$$

$$\tilde{\eta}_{1I} = \sqrt{2}\sigma_1k_{1I}\beta(t)x - 2\sqrt{2}k_{1I}\sigma_1^3\sigma_2 \int \beta^2(t)dt + (k_{1R}^2 - k_{1I}^2)\sigma_1^2 \int \beta^2(t)dt, \quad (13e)$$

and

$$\phi(x, t) = \left(-\frac{\dot{\beta}(t)}{2\beta(t)}x^2 + 2\sigma_1^2\sigma_2(\beta(t)x - \sigma_2\sigma_1^2 \int \beta^2(t)dt) \right), \quad (13f)$$

where the overdot denotes d/dt . All other parameters are given below Eq. (A.1) in the appendix. The mesh plot of evolution of a single oscillating non-autonomous bright soliton is shown in Fig. 4.

In this case, we consider the nonlinearity coefficient to be time-dependent and include the external potential for studying the soliton dynamics. For this purpose, we choose two types of time-dependent nonlinearity coefficients in terms of hyperbolic functions discussed in the previous section. Figs. 4(a)-4(b) show the matter wave soliton compression for the choice $\beta(t) = a_0 + \tanh(\rho t + \delta)$. At time $t \rightarrow 0$, the amplitude and width of the soliton is lower and wider. As time goes on, the amplitude is gradually increased and the pulse width is narrowed down (see time $t \rightarrow 15$). Note that the velocity of the oscillating soliton is strongly affected by the nature of the time-dependent nonlinearity.

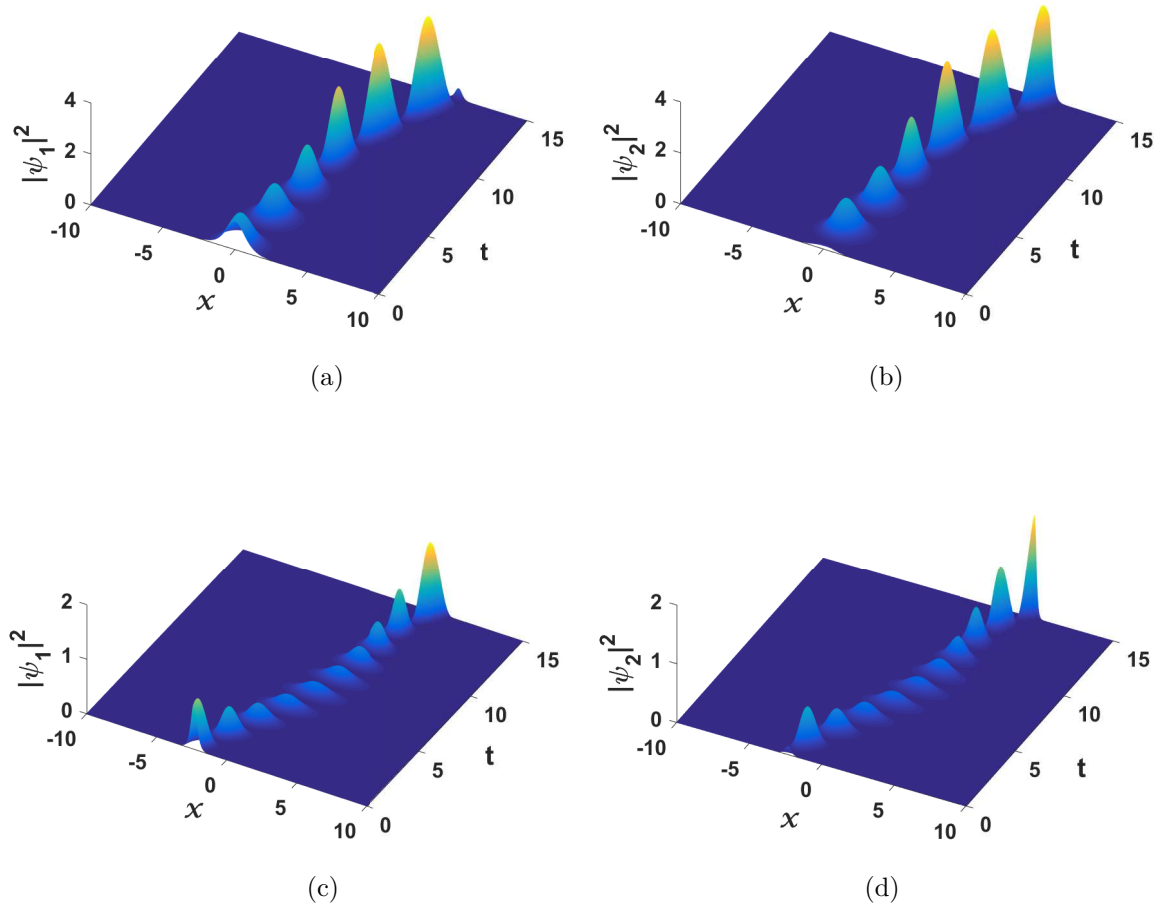


Figure 4. Time-dependent nonlinearity coefficient $\beta(t)$ and presence of external potential (top and bottom row panels). Panels (a) and (b) correspond to values of parameters of $\beta = a_0 + \tanh(\rho t + \delta)$, $k_{1I} = 0.2$, $\rho = 0.4$, $\sigma_1 = 0.8$, $\delta = -3$, $\chi = 1.2$, $a_0 = 2$, and $\sigma_2 = 0$, whereas (c) and (d) correspond to values of parameters $\beta = a_0 + \cosh(\rho t + \delta)$, $k_{1I} = 0.5$, $\rho = 0.45$, $\delta = -3$, $\sigma_1 = 0.2$, $\chi = 2$, $a_0 = 2$, and $\sigma_2 = 0$. All other values of soliton parameters are same as given in Figs. 3(a)-3(c).

Next, we consider the form of time-dependent nonlinearity coefficient as $\beta(t) = a_0 + \cosh(\rho t + \delta)$. In this case the soliton is oscillating and the amplitude is higher at $t = 0$ and at $t = 15$. But in between the amplitude is lower. Note that the central position of the soliton also oscillates periodically. We view this as an oscillating soliton cradle. This is clearly sketched in Figs. 4(c)-4(d).

5.2. Bright two-soliton solution and soliton collision

(i) Brief revisit of collision in the Manakov system:

The soliton solution of Manakov system (8) is described by the two-soliton solution given in appendix (see Eq. (A.2)). The nature of the two soliton collision is shown in Figs. 5(a)-5(b). It shows the shape changing (energy sharing) collision of solitons of

system (8) [35]. Here, S_1 and S_2 denote the first and second soliton, respectively. In the $Q_1(X, T)$ component the condensate density of soliton S_1 gets suppressed after collision while there is an enhancement in that of second soliton S_2 . The reverse scenario takes place in the $Q_2(X, T)$ component. See Ref. [42] for a review of this energy sharing collision.

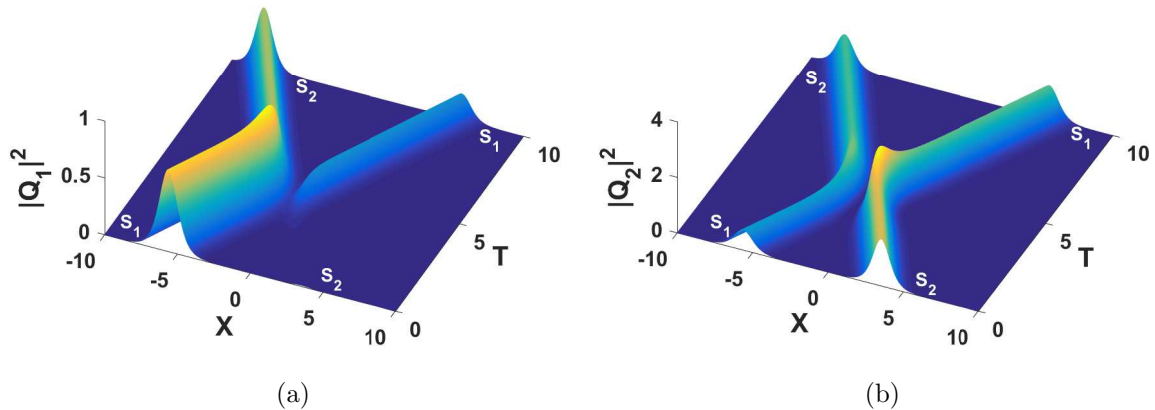


Figure 5. Panels (a)-(b): Shape changing/energy sharing collision of Manakov system (8) with parameters $\alpha_1^{(1)} = \alpha_1^{(2)} = \alpha_2^{(1)} = 0.002$, $\alpha_2^{(2)} = 0.01 + 0.025i$, $k_1 = -1.2 + 0.5i$, and $k_2 = 1.3 - 0.5i$.

(ii) Breather production in soliton collision

In this case, the two-soliton solution for constant nonlinearity parameter ($\beta(t) = 1$) and in the absence of external potential ($V_{\text{ext}}(x, t) = 0$) corresponding to a homogeneous condensate is given by

$$\psi_1(x, t) = \frac{1}{D} \left(\cos(\chi t) G_1 - i \sin(\chi t) G_2 \right), \quad (14a)$$

$$\psi_2(x, t) = \frac{1}{D} \left(-i \sin(\chi t) G_1 + \cos(\chi t) G_2 \right), \quad (14b)$$

where G_1 , G_2 , and D are defined in Eqs. (A.3 and A.4) in the appendix. Here, the form of η_i , $i = 1, 2$, as given in appendix is redefined as $\eta_i = k_i(x + ik_i(t/2))$. The top and middle row panels of Fig. 6 show elastic and energy sharing/shape changing collision of breathing solitons behaviour of system (2), respectively. These figures show that the Rabi coupling induces soliton oscillations which are spatially localized. Such breathing solitons can also be viewed as Ma-breathers. Particularly, panels 6(a)-6(b) show elastic collision of oscillating solitons for the Rabi coupling parameter $\chi = 2$. Figs. 6(c)-6(d) show the shape changing collision of bright solitons in the presence of Rabi coupling. This Rabi coupling affects the switching dynamics significantly. We note that due to the Rabi effect the oscillation in soliton S_1 is completely suppressed before interaction while it reappears after interaction whereas soliton S_2 exhibits oscillation before and after interaction. Another important effect one can notice is that in both the components the switching nature is same. That is, soliton S_1 gets enhanced after interaction. Meanwhile, the soliton S_2 which is completely suppressed before soliton collision in the Manakov case now reappears with significant amplitude and executes periodic oscillations in the ψ_1 component.

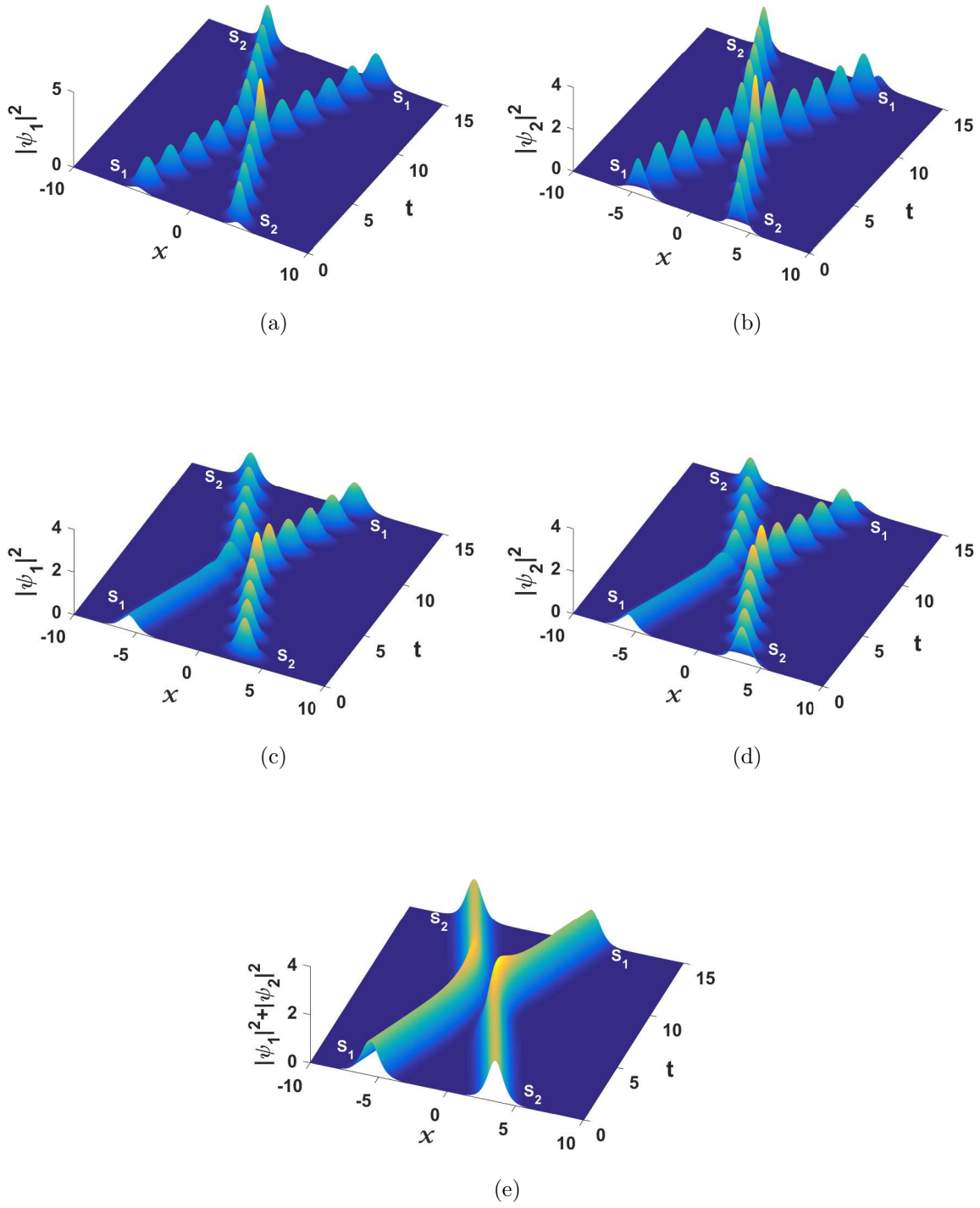


Figure 6. Panels (a)-(b): Elastic collision of oscillating solitons with $\alpha_1^{(1)} = \alpha_2^{(1)} = 0.002$, $\alpha_2^{(2)} = \alpha_1^{(2)} = 0.005i$, $k_1 = -1.4 + 0.5i$, and $k_2 = 1.6 - 0.5i$, $\beta = 1$, and $\chi = 2$. Shape changing collision of oscillating solitons (c)-(d) with $\chi = 2$ and other parameters are same as given in Fig. 5. Panel (e) shows the conservation of energy during shape changing soliton collision.

This is contrary to the collision scenario depicted in Fig. 5 where the Rabi coupling

is absent. However, the total energy is conserved during shape changing collision as depicted in Fig. 6(e) even in the presence of Rabi coupling.

(iii) Collision scenario in the presence of time-dependent nonlinearity coefficient $\beta(t)$ and external potential $V_{\text{ext}}(x, t)$:

Next, we focus our study on soliton dynamics in the presence of the two time-varying nonlinearities discussed in Sec. IV and in the presence of an external potential. The general two-soliton solution of the non-autonomous coupled GP system (2) can be written as

$$\begin{pmatrix} \psi_1 \\ \psi_2 \end{pmatrix} = \frac{1}{D} \begin{pmatrix} \cos(\chi t) & -i \sin(\chi t) \\ -i \sin(\chi t) & \cos(\chi t) \end{pmatrix} \begin{pmatrix} G_1 \\ G_2 \end{pmatrix} \varepsilon(t) e^{i\phi(x,t)}. \quad (15)$$

Here, the co-ordinates X and T appear in the expressions of G_1 and D (see appendix) and are redefined as follows: $X = \sqrt{2}\sigma_1 (\beta(t)x - 2\sigma_2\sigma_1^2 \int \beta^2(t)dt)$, $T = \sigma_1^2 \int \beta^2(t)dt$. Figs. 7(a)-7(b) show the shape changing collision of two breathing solitons for $\beta(t)=a_0 + \tanh(\rho t + \delta)$. The density of the breathing soliton S_1 gets enhanced and S_2 is also enhanced after the collision in the ψ_1 component due to the form of the kink nonlinearity. A similar behavior also takes place in the ψ_2 component. Thus, the switching nature of energy sharing collision in the autonomous system with Rabi coupling is affected by the presence of the time dependent nonlinearity in the non-autonomous GP system (2) for this choice of time-dependent nonlinearity and external potential. This clearly indicates that such type of kink-like nonlinearity can be profitably used for soliton amplification by collision. One can note that the separation distance between the solitons before and after interaction is also increased as compared with Fig. 5.

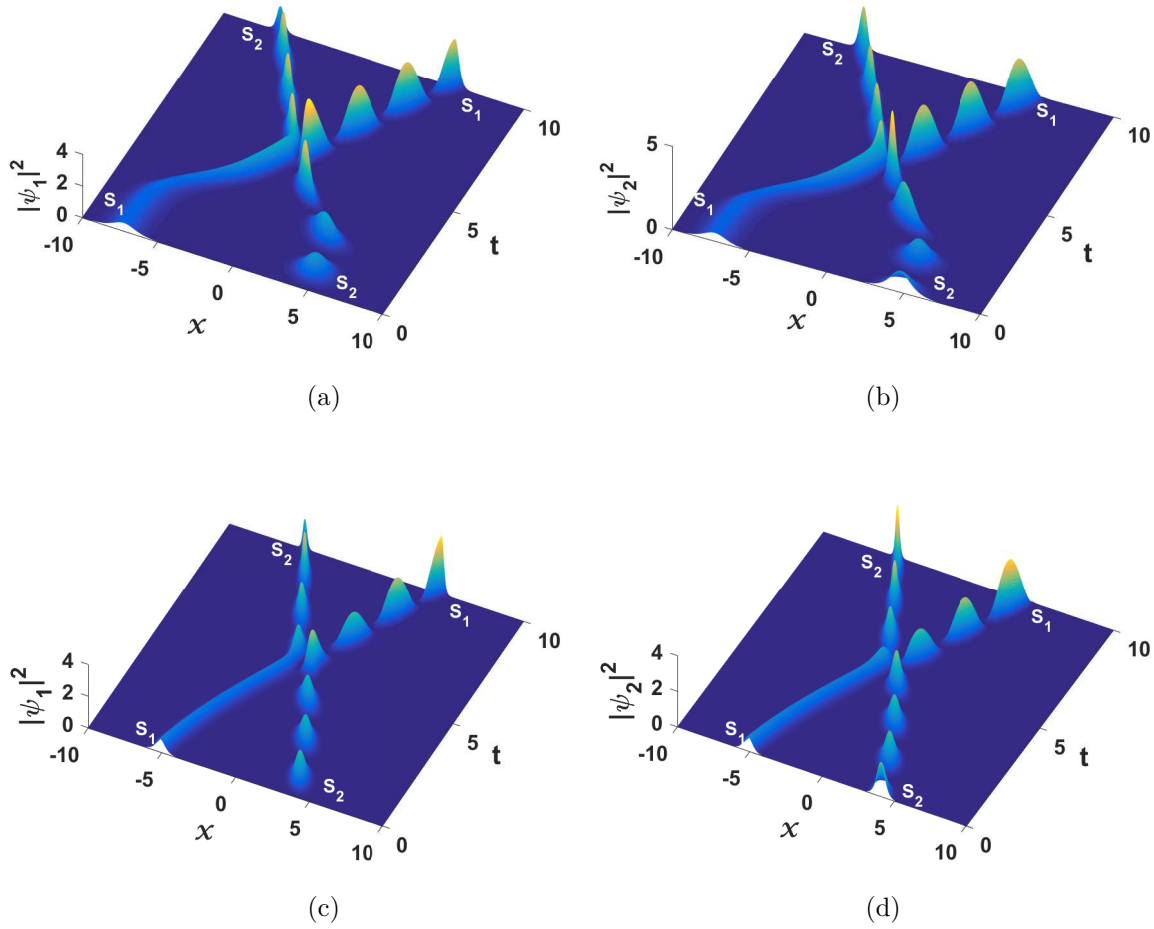


Figure 7. Panels (a)-(b): Shape changing collision of oscillating solitons correspond to values of parameters of $\beta(t) = a_0 + \tanh(\rho t + \delta)$, $\chi = 2$, $\rho = 1.2$, $\sigma_1 = 0.6$, $\sigma_2 = 0$, $a_0 = 2$, and $\delta = -4$. Panels (c)-(d): Shape changing collision with $\beta(t) = a_0 + \cosh(\rho t + \delta)$ with parameters $\rho = 0.35$, $\sigma_1 = 0.4$, $\delta = -1$, $\chi = 2$, $a_0 = 2$, and $\sigma_2 = 0$. All other values are same as given in Fig. 5.

Finally, energy sharing collision of oscillating solitons in non-autonomous GP system (2) with $\beta(t) = a_0 + \cosh(\rho t + \delta)$ is shown in Figs. 7(c)-7(d). We observe that in this case also the energy sharing collision for the non-autonomous GP system (2) with Rabi coupling is altered due to the nature of the nonlinearity coefficient. This nonlinearity can also be used advantageously for soliton amplification purpose. This collision can be viewed as interacting soliton cradles. Here there is a bending in the path of the colliding solitons. However suppression of oscillation in soliton S_1 is still preserved before interaction. The separation distance is left unaffected before and after collision as compared with Figs. 6(c) and 6(d).

6. Stability of non-autonomous bright solitons

Though the autonomous Manakov solitons are found to be stable [40, 43], it is not apparent that the obtained non-autonomous solutions are stable. So our next aim is to investigate the stability of the above discussed non-autonomous solitons. In a recent interesting paper it has been shown that the sufficient and necessary condition for soliton instability and stability is $dP(v)/dv < 0$ and $dP(v)/dv > 0$, respectively [26]. Here, P and v are the normalised momentum and the soliton velocity. In connection with the studies on soliton stability we need the explicit expressions for the norm, soliton position and velocity and normalized momentum. For this purpose, here we calculate the following conserved quantities of non-autonomous system (2). Using the expression (4a) and making use of (13) we find the norm of the soliton is

$$\begin{aligned} N &= \int_{-\infty}^{\infty} \rho \, dx, \\ &= 2\sigma_1^2 \int_{-\infty}^{\infty} k_{1R}^2 \beta(t) \operatorname{sech}^2(k_{1R}\tilde{\omega} + R/2) dx, \\ &= 2\sqrt{2}\sigma_1 k_{1R} \end{aligned} \quad (16)$$

which is time-independent. By requiring the maximum of the condensate density $|\psi_j|^2$, $j = 1, 2$, occurs at the soliton position $x = q$, from (13), we get

$$\sqrt{2}\sigma_1 \left(\beta(t)q - 2\sigma_2\sigma_1^2 \int \beta^2(t)dt \right) = 2k_{1I}\sigma_1^2 \int \beta^2(t)dt - (R/2). \quad (17a)$$

The resulting soliton position at which maximum condensate occurs is given by

$$q(t) = \frac{\zeta}{\sqrt{2}\sigma_1\beta(t)}. \quad (17b)$$

By differentiating the above expression with respect to time ‘t’ one can obtain the velocity of non-autonomous soliton as

$$\dot{q}(t) = \frac{-\beta\dot{\zeta}}{\sqrt{2}\beta^2\sigma_1} + \sqrt{2}\sigma_1\beta(t)k_{1I} + 2\sigma_1^2\sigma_2\beta(t), \quad (17c)$$

where

$$\zeta = \left(2k_{1I}\sigma_1^2 \int \beta^2(t)dt - \frac{R}{2k_{1R}} + 2\sqrt{2}\sigma_1^3\sigma_2 \int \beta^2(t)dt \right). \quad (17d)$$

The top panels [see Fig. 8(a)-8(b)] of Fig. 8 show the evolution of position and velocity of the non-autonomous bright soliton for the nonlinearity parameter $\beta(t) = a_0 + \tanh(\rho t + \delta)$. In this case, the soliton position increases linearly with respect to time except in the jump region of the kink-nonlinearity and in this region it remains almost constant. For this kink nonlinearity, the soliton velocity reaches a negative minimum and attains a constant maximum gradually. The bottom row panels [see Fig. 8(c)-8(d)] of Fig. 8 show the position and velocity of the soliton for the nonlinearity $\beta(t) = a_0 + \cosh(\rho t + \delta)$. In this scenario, there is a shift in the soliton position from negative to positive value as time evolves, whereas the soliton velocity initially takes a smaller value and becomes zero for a significant time period followed by a steep increase. Thus from Figs. 8, it is quite clear that one can engineer the central position and velocity

of the non-autonomous soliton by suitably choosing the temporal modulations of the nonlinearity. This arbitrariness of tuning the soliton position and velocity is not at all possible in its autonomous counterpart.

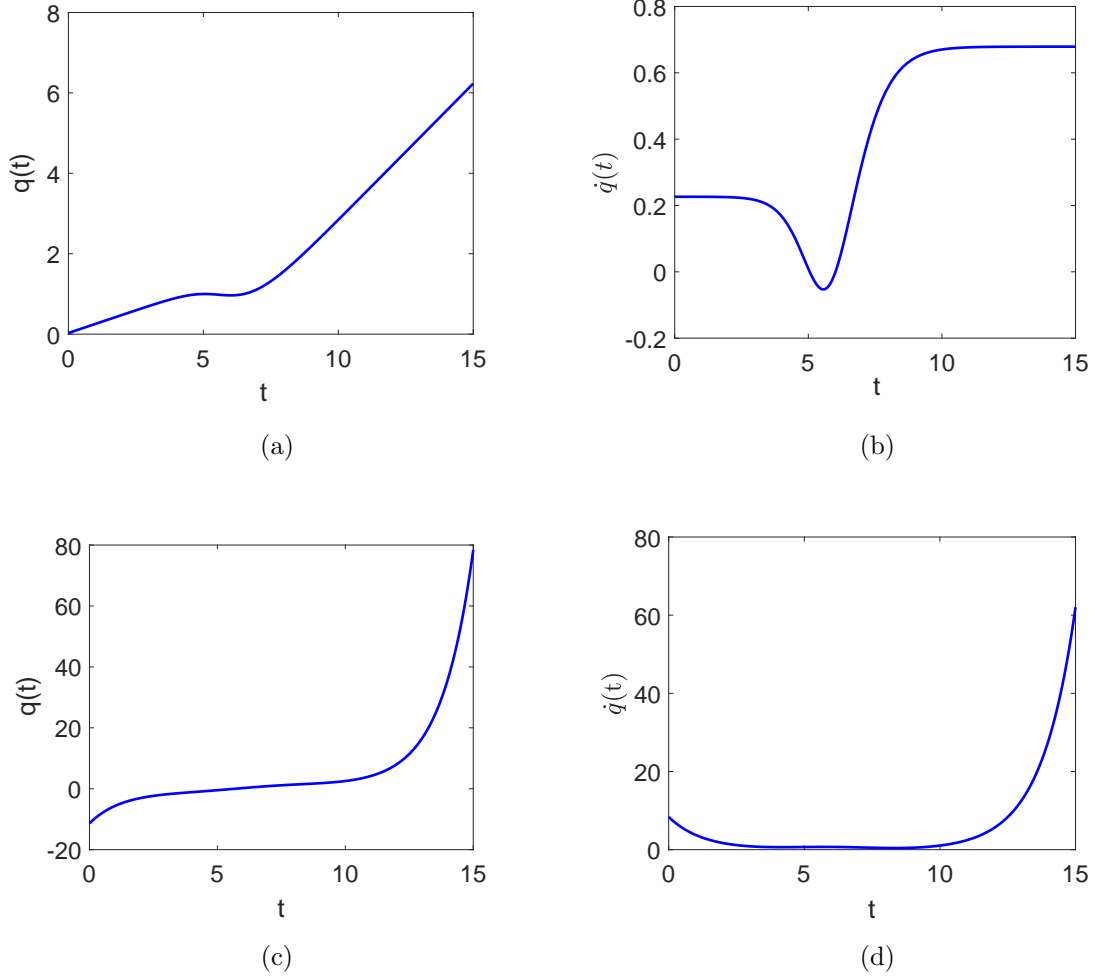


Figure 8. Panels (a)-(d) shows the position and velocity of the bright one soliton solution of system (2) with $\beta(t) = 2 + \tanh(\rho t + \delta)$ and $\beta(t) = 2 + \cosh(\rho t + \delta)$, respectively. The parameters are $k_{1R} = 1$, $k_{1I} = 0.2$, $\alpha_1^{(1)} = 0.5$, $\alpha_1^{(2)} = 0.2i$, $\sigma_1 = 0.8$, $\sigma_2 = 0$, $\delta = -5$, $a_0 = 2$, and $\rho = 0.8$.

The field momentum of soliton p is obtained after substituting the one soliton solution (13) in the following expression:

$$p = \int_{-\infty}^{\infty} j(x, t) dx, \quad (18a)$$

where the current density

$$j(x, t) = 2[-x\dot{\beta} + \sqrt{2}\sigma_1 k_{1I}\beta^2(t) + 2\sigma_1^2\sigma_2\beta^2(t)]k_{1R}^2\sigma_1^2\text{sech}^2(k_{1R}\tilde{\omega} + R/2). \quad (18b)$$

We get the final expression for the momentum current density after substituting $j(x, t)$

in Eq. (18a) as

$$\begin{aligned}
 p &= 4k_{1I}k_{1R}\beta(t)\sigma_1^2 + 4\sqrt{2}k_{1R}\sigma_1^3\sigma_2\beta(t) - \frac{\dot{\beta}}{\beta^2} \left(4\sigma_1^2k_{1I}k_{1R} \int \beta^2(t)dt \right. \\
 &\quad \left. + 4\sqrt{2}k_{1R}\sigma_1^3\sigma_2 \int \beta^2(t)dt - R \right). \tag{19a}
 \end{aligned}$$

So the normalized momentum is given by

$$\begin{aligned}
 P &= \frac{p}{N} = \frac{-\dot{\beta}}{\sqrt{2}\beta^2(t)\sigma_1} \left(2k_{1I}\sigma_1^2 \int \beta^2(t)dt + 2\sqrt{2}\sigma_1^3\sigma_2 \int \beta^2(t)dt - \frac{R}{2k_{1R}} \right) \\
 &\quad + \beta\sigma_1 \left(\sqrt{2}k_{1I} + 2\sigma_1\sigma_2 \right), \tag{19b}
 \end{aligned}$$

$$P = \dot{q}(t). \tag{19c}$$

From (19c) we find $P(v) = v$, where velocity $v = \dot{q}(t)$. Then we get

$$\frac{dP(v)}{dv} = 1. \tag{20}$$

Hence the necessary condition $dP(v)/dv > 0$ for the stability of the soliton is fulfilled. Let us compare the above expressions for position, velocity, and momentum to the scalar NLS system. Here, in vector NLS system the parameters $\alpha_1^{(1)}$ and $\alpha_1^{(2)}$ resulting due to the vector nature of the system (2) influence the position $q(t)$, velocity $\dot{q}(t)$ and hence the momentum $P(t)$ nontrivially.

7. Conclusion

We have studied the dynamics of bright one- and two-solitons in 1D Rabi-coupled BEC with constant and time-dependent nonlinearity coefficients. With the aid of unitary and similarity/lens-type transformations, the 1D non-autonomous GP system (2) is reduced to the standard integrable Manakov system. We present the bright one- and two-soliton solutions of the Manakov system in the appendix. Then by making use of these soliton solutions, the explicit soliton solutions of the non-autonomous GP system (2) are constructed. The dynamics of bright solitons in the non-autonomous GP system is explored for two forms of physically interesting nonlinearity coefficients, namely hyperbolic nonlinearities. From an application point of view, the temporal modulations of the external potentials corresponding to these two choices of time dependent nonlinearities are identified to have a close, rather almost same, resemblance with the superposed Hermite-Gaussian pulses which can be experimentally realized with modern day lasers. This will open up a way in performing experiments on binary condensates to tune the potential to a desirable form. Specifically, we show that in two-soliton case, the Rabi coupling produces breathers during two-soliton interaction. We also point out the interesting fact that due to the Rabi coupling the energy switching scenario in the Manakov system is altered preserving the total energy. The effect of kink-like nonlinearity is to result in a growth in the amplitude of the two colliding solitons after interaction with significant condensate compression. Also, the separation distance

between the solitons, before interaction is increased as compared with the Manakov soliton interaction. Next, the effect of “cosh” type nonlinearity results in a oscillating soliton collision with a complete suppression of oscillation in soliton S_1 before collision in both the components. The central position of the soliton also oscillates periodically during the collision. One can observe for this case, the separation distance between the solitons, before interaction remains the same as that of the Manakov solitons. Finally, for the first time to the best of our knowledge we have addressed analytically the stability of multicomponent non-autonomous bright solitons. Particulary, we have shown that the non-autonomous bright solitons are indeed stable as the rate of change of normalized momentum with respect to velocity is positive (i.e., $dP(v)/dv > 0$). We hope that the results of our study will be of use in the experimental realization of such solitons in binary BECs and will facilitate the understanding of the collisional properties of non-autonomous solitons in the Bose condensate mixtures.

Acknowledgements

The work of T.K. is supported by Science and Engineering Research Board, Department of Science and Technology (DST-SERB), Government of India, in the form of a major research project (File No. EMR/2015/001408). F.G.M. thanks Alexander von Humboldt-Foundation for travel support.

Appendix A. One- and two- soliton solutions of the integrable Manakov system (8)

Appendix A.1. Bright one-soliton solution

The bright one-soliton solution of equation (8) reads as [34, 35]

$$Q_j(X, T) = A_j k_{1R} \operatorname{sech}\left(k_{1R}\omega + \frac{R}{2}\right) e^{i\eta_{1I}}, \quad j = 1, 2, \quad (\text{A.1})$$

where $\omega = X - 2k_{1I}T$, $\eta_{1I} = k_{1I}X + (k_{1R}^2 - k_{1I}^2)T$, $k_1 = k_{1R} + ik_{1I}$, $R = \log\left[\frac{(|\alpha_1^{(1)}|^2 + |\alpha_1^{(2)}|^2)/(k_1 + k_1^*)^2}{\sqrt{|\alpha_1^{(1)}|^2 + |\alpha_1^{(2)}|^2}}\right]$, $A_1 = \frac{\alpha_1^{(1)}}{\sqrt{|\alpha_1^{(1)}|^2 + |\alpha_1^{(2)}|^2}}$, $A_2 = \frac{\alpha_1^{(2)}}{\sqrt{|\alpha_1^{(1)}|^2 + |\alpha_1^{(2)}|^2}}$ with $|A_1|^2 + |A_2|^2 = 1$. Here, suffices R and I denote the real and imaginary parts.

Appendix A.2. Bright two-soliton solution

The bright two-soliton solution of equation (8) is given by [34, 35]

$$Q_j(X, T) = \frac{G_j}{D}, \quad j = 1, 2, \quad (\text{A.2})$$

where

$$G_j = \alpha_1^{(j)} e^{\eta_1} + \alpha_2^{(j)} e^{\eta_2} + e^{\eta_1 + \eta_2 + \eta_1^* + \delta_{1j}} + e^{\eta_1 + \eta_2 + \eta_2^* + \delta_{2j}}, \quad j = 1, 2, \quad (\text{A.3})$$

$$D = 1 + e^{\eta_1 + \eta_1^* + R_1} + e^{\eta_1 + \eta_2^* + \delta_0} + e^{\eta_2 + \eta_1^* + \delta_0^*} + e^{\eta_2 + \eta_2^* + R_2} + e^{\eta_1 + \eta_1^* + \eta_2 + \eta_2^* + R_3}, \quad (\text{A.4})$$

where, $\eta_i = k_i(X + ik_iT)$, $e^{\delta_0} = \kappa_{12}/(k_1 + k_2^*)$, $e^{R_1} = \kappa_{11}/(k_1 + k_1^*)$, $e^{R_2} = \kappa_{22}/(k_2 + k_2^*)$, $e^{R_3} = |k_1 - k_2|^2/(k_1 + k_1^*)(k_2 + k_2^*)|k_1 + k_2^*|^2$, $e^{\delta_{1j}} = (k_1 - k_2)(\alpha_1^{(j)}\kappa_{21} - \alpha_2^{(j)}\kappa_{11})/(k_1 + k_1^*)(k_1^* + k_2)$, $e^{\delta_{2j}} = (k_2 - k_1)(\alpha_2^{(j)}\kappa_{12} - \alpha_1^{(j)}\kappa_{22})/(k_2 + k_2^*)(k_1 + k_2^*)$, $e^{\delta_{2j}} = |k_1 - k_2|^2(\kappa_{11}\kappa_{22} - \kappa_{12}\kappa_{21})/(k_2 + k_2^*)(k_1 + k_1^*)|k_1 + k_2^*|^2$, and $\kappa_{il} = \sum_{n=1}^2 \alpha_i^{(n)}\alpha_l^{(n)*}/(k_i + k_l^*)$, $i, l = 1, 2$.

References

- [1] Pethick C J and Smith H, *Bose-Einstein Condensation in Dilute Gases* (Cambridge University Press, 2002); Kevrekidis P G, Frantzeskakis D J and Carretero-González R, *Emergent Nonlinear Phenomena in Bose-Einstein Condensates: Theory and Experiment* (Springer-Verlag, Heidelberg, 2008).
- [2] Denschlag J, Simsarian J E, Feder D L, Clark C W, Collins L A, Cubizolles J, Deng L, Hagley E W, Helmerson K, Reinhardt W P, Rolston S L, Schneider B I and Phillips W D 2000 Science **287** 97; Khaykovich L, Schreck F, Ferrari G, Bourdel T, Cubizolles J, Carr L D, Castin Y and Salomon C 2002 Science **296** 1290.
- [3] Burger S, Bongs K, Dettmer S, Ertmer W, Sengstock K, Sanpera A, Shlyapnikov G V and Lewenstein M 1999 Phys. Rev. Lett. **83** 5198.
- [4] Busch Th and Anglin J R 2001 Phys. Rev. Lett. **87** 010401.
- [5] Matthews M R, Anderson B P, Haljan P C, Hall D S, Wieman C E and Cornell E A 1999 Phys. Rev. Lett. **83** 2498; Svidzinsky A A and Fetter A L 2000 Phys. Rev. A **62** 063617.
- [6] Engels P, Atherton C and Hofer M A 2007 Phys. Rev. Lett. **98** 095301.
- [7] Leslie L S, Hansen A, Wright K C, Deutsch B M and Bigelow N P 2009 Phys. Rev. Lett. **103** 250401.
- [8] Cornish S L, Thompson S T and Wieman C E 2006 Phys. Rev. Lett. **96** 170401.
- [9] Cornish S L, Claussen N R, Roberts J L, Cornell E A and Wieman C E 2000 Phys. Rev. Lett. **85** 1795.
- [10] Köhler T, Góral K and Julienne P S 2006 Rev. Mod. Phys. **78** 1311.
- [11] Li J, Sun K and Chen X 2016 Sci. Rep. **6** 38258; Kengne E, Shehou A and Lakhssassi A 2016 Eur. Phys. J. B **89** 78; Ding C Y, Zhang X F, Zhao D, Luo H G and Liu W M 2011 Phys. Rev. A **84** 053631; Xue J K 2005 J. Phys. B: At. Mol. Opt. Phys. **38** 3841.
- [12] Kanna T, Babu Mareeswaran R, Tsitoura F, Nistazakis H E and Frantzeskakis D J 2013 J. Phys. A: Math. Theor. **46** 475201.
- [13] Gaul C, Díaz E, Lima R P A, Domínguez-Adame F and Müller C A 2011 Phys. Rev. A **84** 053627; Díaz E, Mena A G, Asakura K and Gaul C 2013 Phys. Rev. A **87** 015601.
- [14] He J S, Charalampidis E G, Kevrekidis P G and Frantzeskakis D J 2014 Phys. Lett. A **378** 577; Bludov Yu V, Konotop V V and Akhmediev N 2009 Phys. Rev. A **80** 033610.
- [15] Matthews M R, Anderson B P, Haljan P C, Hall D S, Holland M J, Williams J E, Wieman C E and Cornell E A 1999 Phys. Rev. Lett. **83** 3358.
- [16] Nistazakis H E, Rapti Z, Frantzeskakis D J, Kevrekidis P G, Sodano P and Trombettoni A 2008 Phys. Rev. A **78** 023635.
- [17] Merhasin I M, Malomed B A and Driben R 2005 J. Phys. B: At. Mol. Opt. Phys. **38** 877.
- [18] Smerzi A, Trombettoni A, Lopez-Arias T, Fort C, Maddaloni P, Minardi F and Inguscio M 2003 Eur. Phys. J. B **31** 457 (2003).
- [19] Hamner C, Zhang Y, Chang J J, Zhang C and Engels P 2013 Phys. Rev. Lett. **111** 264101.
- [20] Qu C, Tylutki M, Stringari S and Pitaevskii L P 2017 Phys. Rev. A **95** 033614.
- [21] Liu C F, Lu M and Liu W Q 2012 Phys. Lett. A **376** 188.
- [22] Son D T and Stephanov M A 2002 Phys. Rev. A **65** 063621.
- [23] Tylutki M, Pitaevskii L P, Recati A and Stringari S 2016 Phys. Rev. A **93** 043623.
- [24] Usui A and Takeuchi H 2015 Phys. Rev. A **91** 063635.
- [25] Aftalion A and Mason P 2016 Phys. Rev. A **94** 023616.

- [26] Quintero N R, Mertens F G and Bishop A R 2015 *Phy. Rev. E* **91** 012905.
- [27] Roberts J L, Claussen N R, Burke J P, Greene Jr., C H, Cornell E A and Wieman C E 1998 *Phys. Rev. Lett.* **81** 5109.
- [28] Chin C, Grimm R, Julienne P and Tiesinga E 2010 *Rev. Mod. Phys.* **82** 1225.
- [29] Hamner C, Chang J J, Engels P and Hofer M A 2011 *Phys. Rev. Lett.* **106** 065302; Middelkamp S, Chang J J, Hamner C, Carretero-González R, Kevrekidis P G, Achilleos V, Frantzeskakis D J, Schmelcher P and Engels P 2011 *Phys. Lett. A* **375** 642; Yan D, Chang J J, Hamner C, Kevrekidis P G, Engels P, Achilleos V, Frantzeskakis D J, Carretero-González R and Schmelcher P 2011 *Phys. Rev. A* **84** 053630.
- [30] Thalhammer G, Barontini G, De Sarlo L, Catani J, Minardi F and Inguscio M 2008 *Phys. Rev. Lett.* **100** 210402; Papp S B, Pino J M and Wieman C E 2008 *Phys. Rev. Lett.* **101** 040402.
- [31] Deconinck B, Kevrekidis P G, Nistazakis H E and Frantzeskakis D J 2004 *Phys. Rev. A* **70** 063605.
- [32] Serkin V N, Hasegawa A and Belyaeva T L 2007 *Phys. Rev. Lett.* **98** 074102.
- [33] Belmonte-Beitia J, Pérez-García V M, Vekslerchik V and Konotop V V 2008 *Phys. Rev. Lett.* **100** 164102; He X-G, Zhao D, Li L and Luo H-G 2009 *Phys. Rev. E* **79** 056610; Yang Z-Y, Zhao L-C, Zhang T, Feng X-Q and Yue R-H 2011 *Phys. Rev. E* **83** 066602; Yan Z and Jiang D 2012 *Phys. Rev. E* **85** 056608.
- [34] Radhakrishnan R, Lakshmanan M and Hietarinta J 1997 *Phys. Rev. E* **56** 2213.
- [35] Kanna T and Lakshmanan M 2003 *Phys. Rev. E* **67** 046617.
- [36] Steiglitz K 2000 *Phys. Rev. E* **63** 016608.
- [37] Kanna T, Babu Mareeswaran R and Sakkaravarhi K 2014 *Phys. Lett. A* **378** 158.
- [38] McDonald G D, Kuhn C C N, Hardman K S, Bennetts S, Everitt P J, Altin P A, Debs J E, Close J D and Robins N P 2014 *Phys. Rev. Lett.* **113** 013002.
- [39] Akhmediev N, Królikowski W and Snyder A W 1998 *Phys. Rev. Lett.* **81** 4632.
- [40] Kanna T and Lakshmanan M 2001 *Phys. Rev. Lett.* **86** 5043.
- [41] Pollack S E, Dries D, Junker M, Chen Y P, Corcovilos T A and Hulet R G 2009 *Phys. Rev. Lett.* **102** 090402; Pollack S E, Dries D, Hulet R G, Magalhaes K M F, Henn E A L, Ramos E R F, Caracanhas M A and Bagnato V S 2010 *Phys. Rev. A* **81** 053627; Regal C A, Greiner M and Jin D S 2004 *Phys. Rev. Lett.* **92** 040403.
- [42] Kanna T, Sakkaravarthi K and Vijayajayanthi M 2015 *Pramana J. Physics* **85** 881.
- [43] Kockaert P and Haelterman M 1999 *J. Opt. Soc. Am. B* **16** 732.